Investigation of the effect of zinc precursors onto structural, optical and electrical properties of CBD deposited ZnS thin films

Rajeshkumar P Khatri[1], Amitkumar J Patel[2]

[1]Department of Physics, Gujarat Technological University, Ahmedabad 382424, Gujarat, India
[2]Department of Applied Science, Faculty of Physics, Government Engineering College, Godhra, Panchmahal 389001, Gujarat, India

rajukhatri_222@yahoo.co.in

Zinc sulfide (ZnS) thin films were deposited onto microscopic silica slides through the cost-effective chemical bath deposition (CBD) method. The optimized bath parameters were: 25 ml of 0.1 M zinc precursors ($ZnCl_2$, $Zn(CH_3COO)_2$, $ZnSO_4$), 25 ml of 1 M thiourea and 3 ml of 3.75 M triethanolamine (TEA). The effects of different zinc precursors ($ZnCl_2$, $Zn(CH_3COO)_2$, $ZnSO_4$) on the growth mechanism of ZnS thin film were investigated using thermal, structural, morphological, optical and electrical studies. The XRD pattern has shown Miller indexing peaks corresponding to the hexagonal phase of as-grown ZnS thin film with the estimated grain size of $22 - 27$ nm. The change in physical properties (weight loss) of ZnS powder as a function of temperature was recorded using thermogravimetry (TGA/DTA). Scanning electron microscopy (SEM) revealed the effect of $ZnCl_2$, $Zn(CH_3COO)_2$ and $ZnSO_4$ precursors on growth mechanism. UV/visible optical transmission/absorption spectra displayed the transmittance between 10 to 29 % of as-grown ZnS thin film with a band gap in the range of $4.10 - 4.25$ eV. Photoluminescence (PL) analyses demonstrated broad blue emission around ~ 459 nm was attributed to recombination of electron-hole pair from donor-acceptor trap levels to valance band. Raman spectra of ZnS powder prepared using different zinc precursors were also reported. The values of electrical parameters (resistivity, conductivity, activation energy, Hall coefficient, carrier concentration, mobility) were investigated using the two-point probe method and Hall-effect apparatus.

1. Introduction

Zinc sulfide (ZnS) is the most promising material in the field of sensors [1], solar cell [2] and bio-imaging [3]. It is a wide band gap semiconductor that serves as host materials for various kinds of dopant for luminescence application [4]. In view of the above technological importance, several researchers have made efforts to tailor the physical properties of ZnS thin films using variation in thickness [5], molar concentration [6], heat treatment [7], bath temperature [8] and other possible means. Earlier, M. Cao, et al. [9] and T. Liu, et al. [10] investigated the effect of different zinc salts on crystallographic, morphology and optical properties of CBD deposited ZnS thin films. In earlier reported literatures, there has not been enough investigation with the effect of zinc precursors on the physical properties of ZnS thin films.

ZnS thin film has been developed by various researchers using different chemical and physical deposition methods such as Thermal evaporation [11], Metal-organic chemical vapor deposition (MOCVD) [12], Successive ionic layer adsorption and reaction (SILAR) [13], Chemical bath deposition [14], etc. Among these deposition methods, CBD is simple, cost-effective and ideal for large scale deposition [15]. Using this CBD method, a thin film can be deposited nearly at room temperature through a controlled chemical reaction.

In the present work, authors have tried to deposit CBD-ZnS thin film using triethanolamine (TEA) as a complexing agent since it is a much safer alternative compare to hydrazine hydrate [16]. Moreover, the researchers have investigated the effect of different zinc precursors ($ZnCl_2$, $Zn(CH_3COO)_2$, $ZnSO_4$) on structural, morphological, optical and electrical properties of CBD deposited ZnS thin films.

2. Experimental method

All reagents were received from Fisher Scientific and used without further processing. A high-quality silica slide having dimensions $75 \times 26 \times 1$ mm^3 is used as substrate. The cleaning procedure and detailed process of film deposition are reported in our earlier literature [17]. The only difference in the present work is that we deposited three different samples using three different precursors instead of zinc chloride, as reported in earlier work. The optimized molar concentration and volume of precursors for the growth of ZnS thin films are listed in Table 1. The pre-cleaned silica substrate is inserted vertically into the reaction bath. The bath temperature was adjusted to 70 $^\circ$C and deposition was carried for 2 hours. The simplified layout of the chemical bath deposition method is represented in Fig. 1.

TABLE 1. Molar concentration and volume of precursors for the growth of ZnS thin films by CBD method

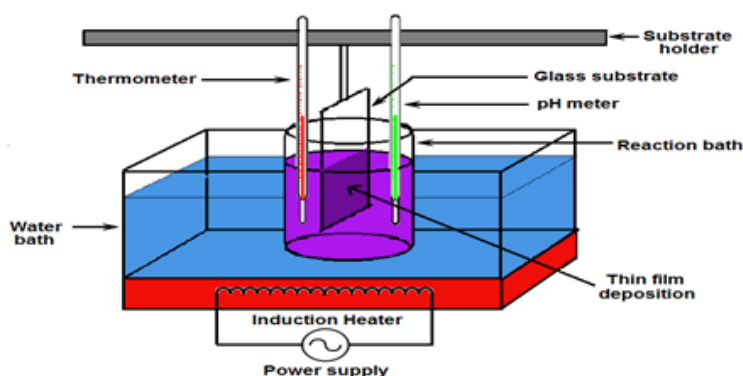| Thin film	Molar concentration and volume of precursors			
	zinc precursor	thiourea	Triethanolamine (TEA)	Ammonia
ZnS–Cl	25 ml of 0.1 M $ZnCl_2$	25 ml of 1 M	3 ml of 3.75 M	2 ml of 13.4 M
ZnS–Ac	25 ml of 0.1 M $Zn(CH_3COO)_2$	25 ml of 1 M	3 ml of 3.75 M	2 ml of 13.4 M
ZnS–SO	25 ml of 0.1 M $ZnSO_4$	25 ml of 1 M	3 ml of 3.75 M	2 ml of 13.4 M

FIG. 1. Simplified layout of Chemical Bath Deposition Method

After the deposition, the film is taken out from the bath and dipped into de-ionized water to remove loosely bound ZnS powder that adheres to the film. ZnS thin films deposited using $ZnCl_2$, $Zn(CH_3COO)_2$ and $ZnSO_4$ were labeled as ZnS–Cl, ZnS–Ac and ZnS–SO, respectively for the sake of analysis.

The deposited ZnS thin films were analyzed using various instruments without annealing treatment. The alteration in physical properties as a function of temperature was obtained using thermogravimetry (METTLER TOLEDO). The Miller indices (h k l) for diffracting planes for the given structure of the thin film was evaluated by grazing incident X-ray diffraction (GIXRD) spectrometer (PANalytical Empyrean) using CuKα radiations (wavelength = 0.15406 nm) for 2θ values over $20 - 60^\circ$. X-ray was impinging at angle 0.5° and a detector was moving in the step of 0.01° with a collection time of 7 s. The surface morphology was characterized using the field emission scanning electron microscope (JEOL JSM-6010LA). The stoichiometric composition of films was analyzed by energy dispersive X-ray analysis (EDX) using an EDX detector which is available as an add-on attachment with the scanning electron microscope (JEOL JSM-5610LV) with Inca software. In order to find the permitting light wavelengths for thin films, transmission/reflectance spectra were recorded as a function of wavelengths using UV/VIS/NIR spectrophotometer (Perkin Elmer Lambda 19). The Raman scattering measurement (vibrational phonon modes) was investigated at room temperature using a Raman microscope (RENISHAW Invia) with 514 nm (20 mW) argon ion excitation source. Photoluminescence spectra were registered with Perkin Elmer spectro-fluoro-photometer using 280 nm excitation wavelength. A self-made two probe resistivity measurement equipment and Hall-effect apparatus were used to find the correlation between different electrical parameters.

3. Results and discussion

3.1. Thermal analysis

In order to perform thermal analysis of the obtained samples, the as-deposited ZnS powders are collected by scratching the surface of deposited silica substrates. The analysis of the thermal behavior of scratched as-deposited ZnS powders were carried out using differential thermal analysis (DTA) and thermogravimetric analysis (TGA) in an ambient environment with temperature in the range of 30 – 900 °C. During measurements, the temperature was increased at a rate of 30 °C/min. DTA and TGA curves for ZnS–Cl, ZnS–Ac, and ZnS–SO powder are shown in Fig. 2.
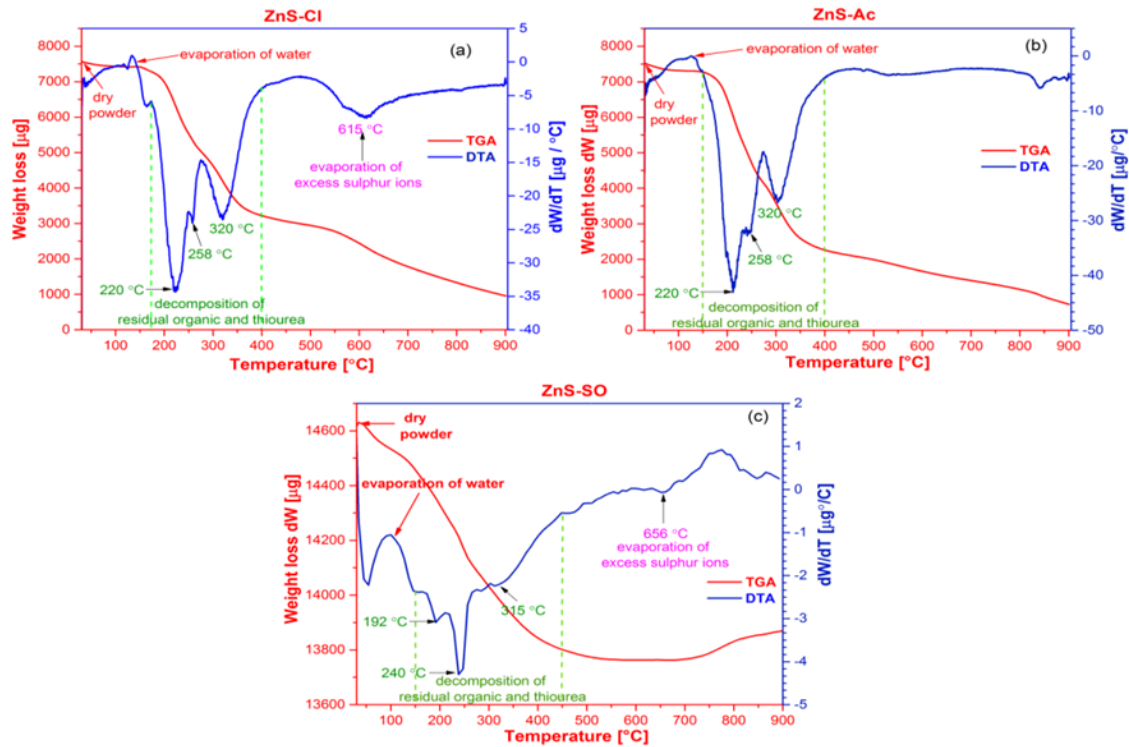

FIG. 2. TGA and DTA curves for ZnS powders grown by CBD method using different zinc precursors: (a) ZnS–Cl; (b) ZnS–Ac (c) ZnS–SO

The TGA curve indicates that all the as-grown samples of ZnS lose weight from 30 to 150 °C as a result of absorbed water vapor evaporation. The decomposition of residual organics and TEA leads to second weight loss between 150 – 450 °C. It is also confirmed by a series of endothermic peaks between temperature ranges 150–450 °C in DTA sketches, as shown in Fig. 2. The endothermic peak at 615 °C in the case of ZnS–Cl and 656 °C in the case of ZnS–SO could be attributed to the evaporation of excess residual sulfur ions from the sample [18].

3.2. Structural analysis

The structural information of ZnS thin film was obtained using grazing incident X-ray diffraction (GIXRD) with CuKα radiation with scan range 20 – 60°. GIXRD can reduce the signal contribution from the substrate and improve the signal from the thin film. X-ray diffractogram of as-grown ZnS thin film prepared using different zinc precursors (ZnCl$_2$, Zn(CH$_3$COO)$_2$ and ZnSO$_4$) are shown in Fig. 3.

The peaks at 2θ values 31.64°, 34.53°, 36.20°, 47.45° and 56.48° are diffraction angles for planes with Miller indices (1 0 4), (1 0 6), (0 0 10), (1 1 0) and (1 1 8) which satisfies Bragg's equation. The plane (0 0 10) consists more number of atoms resulted in the highest intensity peak. Comparing observed peaks with JCPDS card No. 39-1363 assures hexagonal phase of ZnS thin film.

The particle size of ZnS thin films deposited using different zinc precursors were calculated using the Debye–Scherrer formula as [19]:

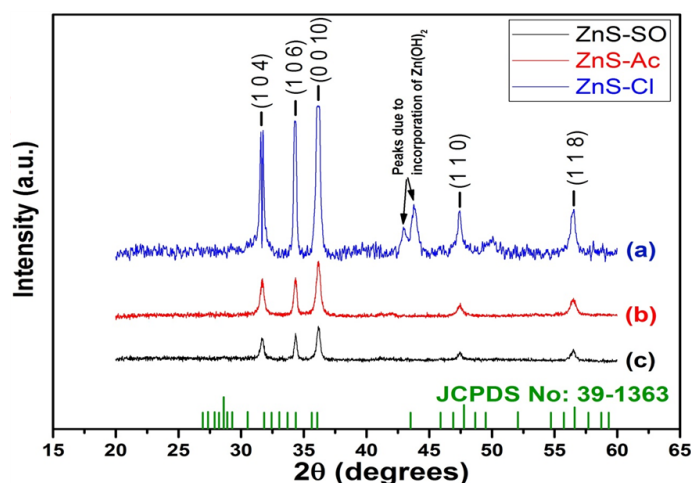$$D = \frac{0.94\lambda}{\beta \cos\theta}, \tag{1}$$

FIG. 3. X-ray diffractogram for as-grown ZnS thin films deposited using different zinc precursors: (a) ZnS-Cl; (b) ZnS-Ac;(c) ZnS-SO

where D is particle size, λ is the wavelength of incident X-ray generally its value is 0.15406 nm for CuKα radiation, β is full width at half maximum (FWHM) for the peak of the plane with Miller indices (h k l) and θ is the angle between the incident beam and (h k l) plane. The particle sizes of as-grown ZnS thin film deposited using different zinc precursors onto the silica substrate are listed in Table 2. From X-ray diffractogram and particle size analysis, it is clearly observed that anions associated with zinc precursors play an important role in the growth chemistry of ZnS thin films. The intermolecular interactions between anions and intermediate complex precursors decide heterogeneous or homogenous growth mechanism for ZnS film growth [10]. In our case, the Cl$^-$ anions favor heterogeneous (ions by ions) growth mechanism and improve the crystallinity of ZnS thin films while SO$_4^{-2}$ and CH$_3$COO$^-$ anions follow homogeneous (clusters by clusters) or mixed growth mechanism for ZnS thin film formation on silica slide. Moreover, two extra peaks are observed in the case of ZnS–Cl thin film at 42.93 and 43.87°, which are likely due to the incorporation of Zn(OH)$_2$ into the film during the growth process [20, 21]. In this case, ZnS film could be formed by the decomposition of thiourea over the surface of intermediate hydroxide cluster Zn(OH)$_2$ rather than nucleate separately in the solution.

TABLE 2. Particle size, thickness, transmittance and band gap of as-grown ZnS thin films deposited using different zinc precursors

Thin film (ZnS thin film)	Particle size (nm)	Thickness (μm)	Avearge Transmittance T (%) ($\lambda > 350$ nm)	Band gap (eV)
ZnS–Cl	27	37 ± 0.2	29	4.10
ZnS–Ac	25	39 ± 0.3	25	4.17
ZnS–SO	22	41 ± 0.2	10	4.25

The thickness of ZnS thin films deposited using different zinc precursors was predicted using the transverse view of SEM images, which are presented in Fig. 4. The observed values of thickness are listed in Table 2. It is apparently clear that the thickness of ZnS thin films was greatly affected by growth rate and hence liberated anions from zinc precursors in solution during growth mechanism.

In order to investigate the effect of zinc precursors onto the surface morphology of as-grown ZnS thin film, micrographs of films were recorded using scanning electron microscope which is shown in Fig. 5. In general, the films deposited by chemical route have uncontrolled growth rate resulted in non-uniform surface.

In the present research, ZnS thin films acquire rough surfaces due to uneven grain growth in different directions. Fig. 5(a) shows ZnS–Cl film has a smooth, compact surface with reduced grain boundaries than other films. The reduction of grain boundaries has a considerable effect on the carrier drift velocity of materials [22]. Fig. 5(c) shows
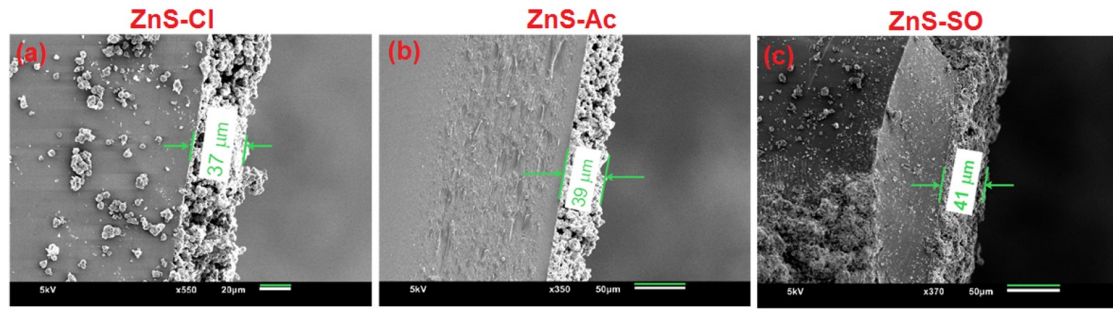
FIG. 4. Transverse view of SEM images for as-grown ZnS thin films deposited using different zinc precursors: (a) ZnS-Cl; (b) ZnS-Ac; (c) ZnS-SO
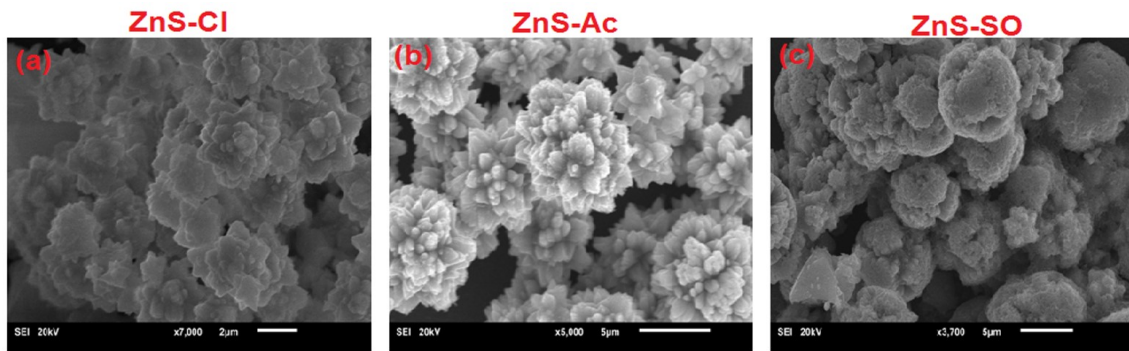

FIG. 5. SEM micrograph of as-grown ZnS thin films deposited using different zinc precursors: (a) ZnS-Cl; (b) ZnS-Ac; (c) ZnS-SO

ZnS–SO films formed by significant spherical clusters with relatively less dense morphology. The reason for this is SO_4^{-2} anions promote homogeneous (clusters by clusters) growth mechanism and ZnS clusters from solution adhere on a silica substrate. Fig. 5(b) shows ZnS–Ac film is relatively less compact than ZnS–Cl with flower-like morphology. In this case, CH_3COO^- anions promote a mixed growth mechanism in the solution for deposition of ZnS thin films.

3.3. Compositional analysis

The elemental composition of ZnS films deposited onto the silica substrate using different zinc precursors was analyzed using EDX spectra and is shown in Fig. 6. The obtained results are listed in Table 3. Because of the low thickness of films and high depth profile of EDX spectrometer, other elements from silica substrate such as O, Mg, Si, and Ca are also detected in the EDX spectra. As seen from Table 3, the atomic ratios of Zn/S are slightly higher than 1 which indicates that the obtained ZnS films are rich in zinc and deficient in sulfur. The difference in the Zn/S ratio is ascribed to different growth mechanisms involved during film formation. The presence of excess zinc in the case of ZnS–Cl films could be due to the presence of $Zn(OH)_2$ [9, 10], which is consistent with our XRD results.

TABLE 3. Elemental composition of as-deposited ZnS thin films from EDX spectra

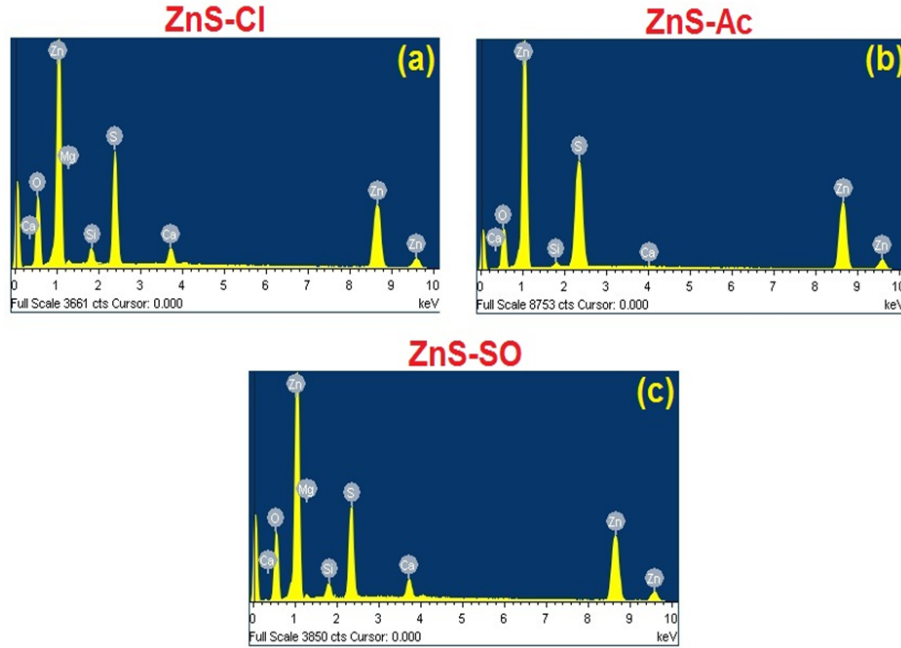| Thin film	Zn (at %)	S (at %)	Other elements (at %)	Zn/S atomic ratio
ZnS–Cl	26.22	22.74	51.04	1.15
ZnS–Ac	25.38	22.58	52.04	1.12
ZnS–SO	24.71	22.45	52.84	1.10

FIG. 6. EDX spectra of as-grown ZnS thin films deposited using different zinc precursors: (a) ZnS-Cl; (b) ZnS-Ac; (c) ZnS-SO

3.4. Optical analysis

The thickness and uniformity of film play a vital role in controlling optical properties like transmittance, absorbance, refractive index, etc. [23]. A film with higher uniformity and the least thickness leads to the high transmission with a sharp absorption edge [24]. Moreover, the energy band gap of the film can be determined from transmission spectra [23].

In the direction to know the effect of zinc precursors on the optical behavior of as-grown ZnS thin films, transmittance and reflectance spectra were noted using UV/VIS/NIR spectrophotometer. Fig. 7 shows the percentage of transmittance and absorbance of CBD-deposited as-grown ZnS thin films with zinc precursor variation. The highest transmittance is observed in ZnS–Cl thin film and lowest in ZnS–SO thin film. It shows low absorption above 350 nm wavelength and abrupt absorption at ~ 310 nm wavelength for all ZnS thin films.
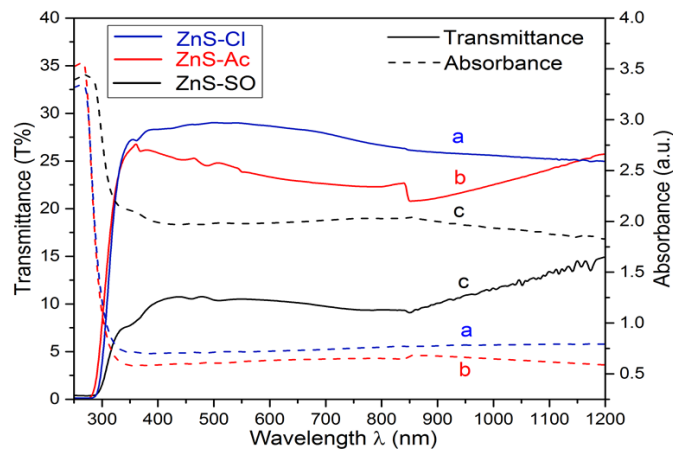

FIG. 7. UV/visible transmittance and absorbance spectra of as-grown ZnS thin films deposited using different zinc precursors: (a) ZnS-Cl; (b) ZnS-Ac; (c) ZnS-SO

Once Transmission/Reflectance data were registered with respect to wavelength, the optical energy band gaps of thin films were evaluated with the help of the formula derived from the theory of inter-band transition of the

semiconductor. The absorption coefficient (α) was determined from absorbance (A) and film thickness (t) by using the relation [25, 26]:

$$\alpha = \frac{2.303 \cdot A}{t}. \tag{2}$$

The theory of inter-band transition shows that at the optical absorption edge, the absorption coefficient (α) varies with the photon energy hν according to [23]:

$$\alpha h\nu = A(h\nu - E_g)^n, \tag{3}$$

where E_g is the optically forbidden energy gap, A is constant and the exponential factor $n = 1/2, 1, 2, 3$ depending on the type of electronic transition in k-space [26]. For direct band gap semiconductor, the exponential factor has value 0.5 and for indirect band gap semiconductor, it has a value of 2. Since ZnS is a direct band gap material, the value of n becomes 0.5:

$$(\alpha h\nu)^2 = A^2(h\nu - E_g). \tag{4}$$

Figure 8 represents the plot of $(\alpha h\nu)^2$ versus $h\nu$ for as-grown ZnS thin film deposited from different zinc precursors. The film's band gap value is obtained by extrapolating the straight-line portion of curves to $\alpha h\nu = 0$ using a computer fitting program in which the intercept value of $h\nu$-axis is band gap value. The calculated band gaps (E_g) for as-grown ZnS films are listed in Table 2. The estimated band gap value of ZnS–Cl, ZnS–Ac and ZnS–SO thin films are found to be 4.10, 4.17 and 4.25 eV, respectively. The tabulated band gap values of ZnS thin films showed that the increase in particle size due to the presence of different anions during the growth mechanism lower the band gap values due to the quantum size effect. Further, the tabulated band gap values of all ZnS thin films are slightly higher than bulk ZnS, which is probably due to the quantum size effect as the grown polycrystalline thin films' grain size is small enough [10, 27].
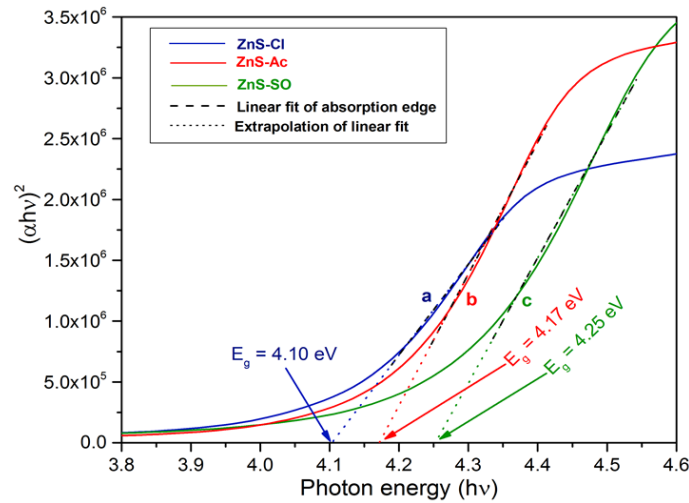

FIG. 8. Plot of $(\alpha h\nu)^2$ versus $h\nu$ for as-grown ZnS thin films deposited using different zinc precursors: (a) ZnS-Cl; (b) ZnS-Ac; (c) ZnS-SO

3.5. Photoluminescence study

The photoluminescence (PL) spectra of as-grown ZnS thin film grown using different zinc precursors under UV excitation is presented in Fig. 9. The intense emission with blue wavelength range is observed in all ZnS thin films, which could be attributed to the recombination of electron-hole pair from donor-acceptor trap levels to the valance band [28]. The stoichiometric difference of ZnS film during the growth mechanism is responsible for various kinds of defect formations. As per EDX analysis, the obtained ZnS films have a Zn/S ratio greater than 1. This stoichiometric deviation leads to excess zinc and a sulfur deficiency which could produce zinc interstitial (Zn_i) and sulfur vacancies (V_S) in ZnS thin film. The broadening of PL spectra around Zn_i was ascribed to various kinds of donor-acceptor pair transitions due to the formation of native defect states into the forbidden gap, which is depicted in Fig. 10.

In the present case, blue emission at ~ 459 nm signifies the involvement of interstitial zinc ions [28]. The spreading of emission spectra of ZnS thin film around blue wavelength is credited to different types of donor-acceptor transitions along with zinc interstitial [28]. The intensity of ZnS–SO is higher than other films and can be ascribed to the hindrance of diffusion of zinc complex precursors onto the silica substrate during growth of film and hence the
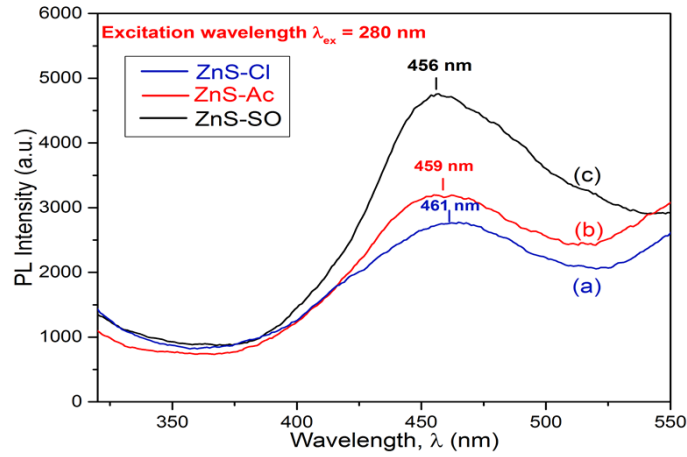
FIG. 9. Emission spectra of as-grown ZnS thin films deposited using different zinc precursors: (a) ZnS-Cl; (b) ZnS-Ac; (c) ZnS-SO
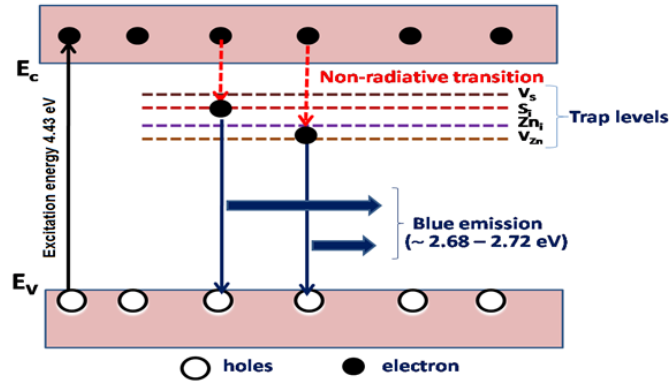

FIG. 10. Energy band diagram of the photoluminescence phenomenon in as-grown ZnS powder grown using different zinc precursors [28]

formation of native defect states. These indicate that anions play a crucial role in defect formation during the growth of thin films.

3.6. Raman study

For 514 nm excitation wavelength, ZnS thin film has low Raman scattering efficiency and is detectable only with film thickness 1 μm or higher [29]. Therefore, the Raman spectra of scratched as-grown ZnS powder (instead of ZnS thin films) prepared using different zinc precursors were recorded using 514 nm excitation wavelength (green excitation) shown in Fig. 11. The peak positioned at 348 cm^{-1} corresponds to the first-order longitudinal optical (LO) mode of ZnS materials. The second-order and third-order LO modes are observed at 697 and 1018 cm^{-1}, respectively. The obtained results are found consistent with the reviewed literature [29]. The intensity of the LO peak is highest for ZnS–Cl and that of the lowest for ZnS–SO. The peak due to the 2LO phonon is absent in ZnS–SO, while a slightly visible peak is observed in ZnS–Ac and ZnS–Cl with an increase in intensity, respectively. This could be due to anions present in zinc precursors affecting the defect chemistry of ZnS thin film during deposition, which influences the vibrational mode of ZnS thin films [29]. The increase in the sharpness of phonon peak represents an improvement in crystallinity [9] which is consistent with the above discussions.

3.7. Electrical measurements

The activation energy, electrical resistivity and conductivity of all ZnS thin films were determined using the two-point probe method. The relation for resistivity with temperature is denoted by [30]:

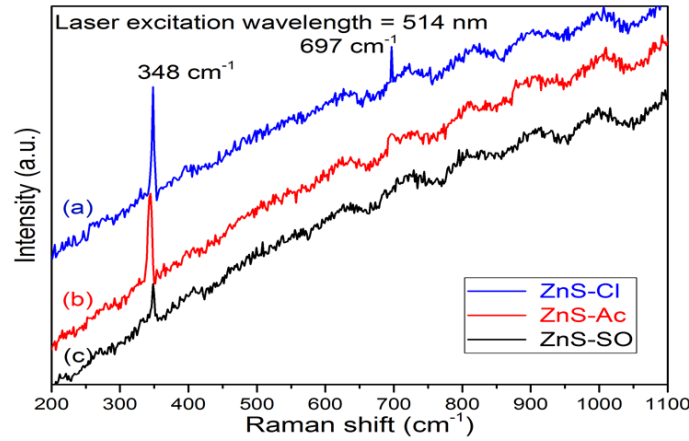$$\log \rho = \frac{E_a}{2.303 \cdot k_B} \left(\frac{1}{T}\right) + \log C, \tag{5}$$

FIG. 11. Raman spectra of as-grown ZnS powders prepared by different zinc precursors: (a) ZnS-Cl; (b) ZnS-Ac; (c) ZnS-SO

where ρ is resistivity (in $\Omega\cdot$cm), E_a is activation energy (in eV), k_B is Boltzmann constant (in eV/K), T is the temperature (in Kelvin) and $\log C$ is constant.

The Hall coefficient, carrier concentration and mobility of thin films were figured out using the relation given below [31]:

$$R_H = \frac{V_H \cdot t}{I \cdot B}, \qquad \eta = \frac{1}{R_H \cdot q}, \tag{6}$$

where R_H is Hall Coefficient (cm^3/C), V_H is Hall Voltage (in volt), I is probe current (in Ampere), t is the thickness (in meter), B is the magnetic field (in Gauss) and η is carrier concentration (in 1/cm^3).

The data for the resistivity measurements were recorded by raising the temperature from 35 to 190 °C. The plot for $\log \rho$ Vs $1000/T$ for ZnS thin film deposited using different zinc precursors is depicted in Fig. 12. The plot of $\log \rho$ versus $1000/T$ gives a straight line whose slope corresponds to E_a/k_B. The calculated values of resistivity, conductivity and activation energy is represented in Table 4. The shallow trap levels are responsible for low activation energy E_{a1} and the deep trap levels are responsible for the high value of activation energy E_{a2} in the case of ZnS–SO thin film [32].
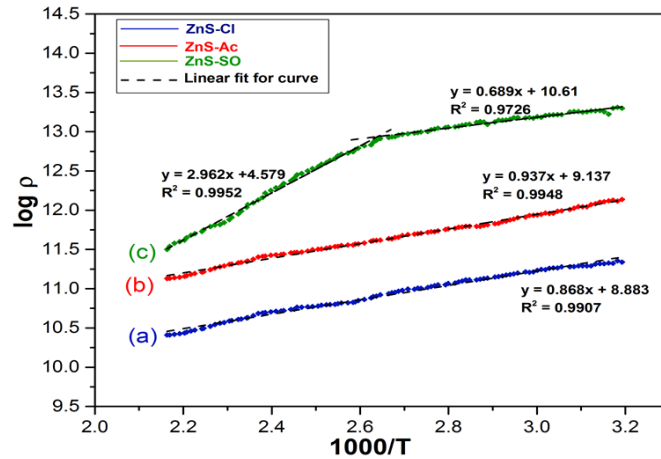

FIG. 12. Plot of $\log \rho$ versus $1000/T$ for as-grown ZnS thin films deposited using different zinc precursors

The Hall effect measurements were recorded by keeping probe current constant and varying magnetic field and measuring corresponding Hall voltage. The sketch for Hall voltage versus magnetic field is outlined in Fig. 13. The calculated values for the Hall coefficient, carrier concentration and mobility are listed in Table 4. The n-type conductivity was observed in all ZnS films irrespective of zinc precursors used. The tabulated values show that ZnS–SO thin film has a high charge density and low conductivity compared to other thin films. The explanation of the observed results is that native defect states are generated during the growth of film act as scattering centers

TABLE 4. Electrical parameter for as-grown ZnS thin films deposited using different zinc precursors: ZnS–Cl (a); ZnS–Ac (b); ZnS–SO (c)

Thin film	Activation energy (eV)		Resistivity ρ (Ω·cm)	Conductivity σ (Ω^{-1}·cm^{-1})	Hall Coefficient RH (cm^3/C)	Carrier concentration η (cm^{-3})	Mobility μ (cm^2/V$_s$)
	E_{a1}	E_{a1}					
ZnS–Cl	0.75	—	2.08×10^4	4.81×10^{-5}	3.48×10^3	1.79×10^{15}	1.68×10^{-1}
ZnS–Ac	0.81	—	1.63×10^4	6.14×10^{-5}	1.71×10^2	3.65×10^{16}	1.05×10^{-2}
ZnS–SO	0.59	2.55	8.52×10^4	1.17×10^{-5}	2.53×10^1	2.47×10^{17}	2.97×10^{-4}

for conduction electrons in the film. So defect chemistry and hence anions associated with zinc precursors play an important role in the electrical transport properties of ZnS thin films. Fig. 14 represents the comparative graph for carrier concentration, conductivity and mobility for ZnS thin films. It reveals from the graph that ZnS-Cl shows a considerable amount of conductivity compared to other samples even though its low carrier concentration. This is due to the high mobility offered by it.
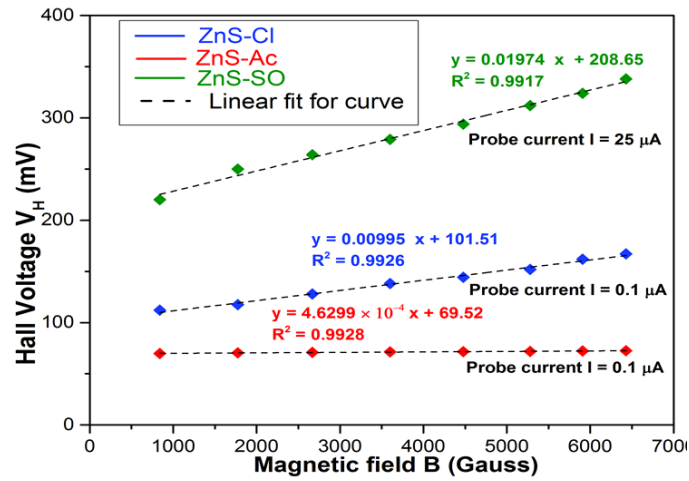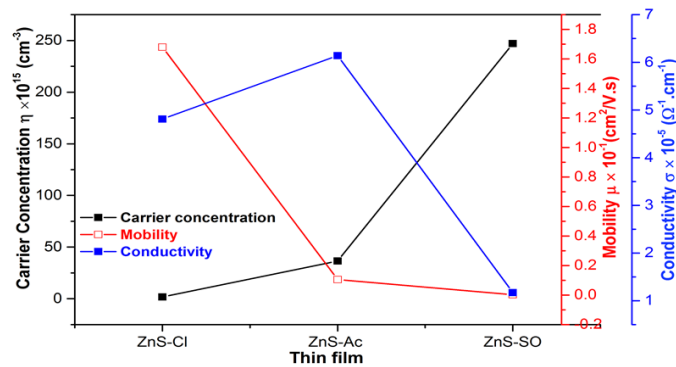

FIG. 13. Plot of Hall voltage VH versus magnetic field B for constant probe current of ZnS thin films deposited using different zinc precursors

FIG. 14. Comparative graph for carrier concentration, mobility and conductivity for as-grown ZnS thin films deposited using different zinc precursors

4. Conclusion

Good quality ZnS thin films have been deposited onto silica substrates using different zinc precursors, thiourea, non-toxic complexing agent triethanolamine (TEA) by optimizing bath parameters. The XRD confirms the hexagonal phase with maximum intensity peak along (0 0 10) plane of as-grown ZnS thin film prepared using different zinc precursors. SEM demonstrates the notable effect of anions of zinc precursors on the growth mechanism of ZnS thin film. Optical measurements demonstrate transmittance varies from 10 to 29 % in the visible region. The band gap increases with a decrease in particle size due to the quantum size effect. The ZnS thin film has higher band gap values than the counter bulk sample in the range of 4.10 – 4.25 eV. The blue emission at ~ 459 nm was obtained by PL spectra under UV excitation. The first-order Raman shift was observed at 348 cm^{-1} in all ZnS films. The Hall-effect apparatus measures carrier concentration of order 10^{15} to 10^{17} e$^-$/cm^3, reflecting the semiconducting nature of ZnS thin film with n-type conductivity. The observed studies show the significant effect of zinc precursors on the transport properties of CBD-ZnS thin films. ZnS thin film deposited using ZnCl$_2$ as precursor material is found to have good carrier mobility amongst all films.

References

[1] Nemade K.R., Waghley S.A. Ultra-violet C absorption and LPG sensing study of zinc sulphide nanoparticles deposited by a flame-assisted spray pyrolysis method. *Journal of Taibah University for Science*, 2016, **10** (3), P. 437–441.

[2] Islam M.M., Ishizuka S., et al. CIGS solar cell with MBE-grown ZnS buffer layer. *Solar Energy Materials & Solar Cells*, 2009, **93**, P. 970–972.

[3] Bujňáková Z., Dutková E. Mechanochemistry of Chitosan-Coated Zinc Sulphide (ZnS) Nanocrystals for Bio-imaging Applications. *Nanoscale Research Letters*, 2017, **12**, 328.

[4] Ben Nasr T., Kamoun N., Guasch C. Structure, surface composition, and electronic properties of zinc sulphide thin films. *Materials Chemistry and Physics*, 2006, **96**, P. 84–89.

[5] Ubale A.U., Kulkarni D.K. Preparation and study of thickness dependent electrical characteristics of zinc sulfide thin films. *Bull. Mater. Sci.*, 2005, **28** (1), P. 43–47.

[6] Yu F-P., Ou S-L., et al. Structural, Surface Morphology and Optical Properties of ZnS Films by Chemical Bath Deposition at Various Zn/S Molar Ratios. *Journal of Nanomaterials*, 2014, **6**, P. 1–7.

[7] Gode F. Annealing temperature effect on the structural, optical and electrical properties of ZnS thin films. *Physica B*, 2011, **406**, P. 1653–1659.

[8] Zein R., Alghoraibi I. Influence of Bath Temperature and Deposition Time on Topographical and Optical Properties of Nanoparticles ZnS Thin Films Synthesized by a Chemical Bath Deposition Method. *Journal of Nanomaterials*, 2019, 1–13.

[9] Cao M., Zhang B.L., Li L. Huang J., et al. Effects of zinc salts on structural and optical properties of acidic chemical bath deposited ZnS thin films. *Materials Research Bulletin*, 2013, **48**, P. 357–361.

[10] Liu T., Ke H., et al. Effect of four different zinc salts and annealing treatment on growth, structural, mechanical and optical properties of nanocrystalline ZnS thin films by chemical bath deposition. *Materials Science in Semiconductor Processing*, 2014, **26**, P. 301–311.

[11] Gurin N.T., Sabitov O.Y., Afanas'ev A.M. Characteristics of surface states at the insulator-semiconductor interface in the thin-film electroluminescent structures based on ZnS:Mn. *Semiconductors*, 2010, **44** (4), P. 498–507.

[12] Migita M., Kanehisa O., Shiiki M. Yamamoto H. The Preparation of ZnS:Mn electroluminescent layers by MOCVD using new manganese sources. *Journal of Crystals Growth*, 1988, **93** (1–4), P. 686–691.

[13] Lindroos S., Kanniainen T. Leskela M., Rauhala E. Deposition of manganese-doped zinc sulfide thin films by the successive ionic layer adsorption and reaction (SILAR) method. *Thin Solid Films*, 1995, **263** (1), P. 79–84.

[14] Doña J. M., Herrero J. Process and film characterization of chemical-bath-deposited ZnS thin films. *Journal of The Electrochemical Society*, 1994, **141** (1), P. 205–210.

[15] Oladeji I.O., Chow L., et al. Comparative study of CdS thin films deposited by single, contineous, and multiple dip chemical processes. *Thin Solid Films*, 2000, **359** (2), P. 154–159.

[16] Liu J., Wei A., Zhao Y. Effect of different complexing agents on the properties of chemical-bath-deposited ZnS thin films. *Journal of Alloys and Compounds*, 2014, **588**, P. 228–234.

[17] Khatri R.P., Patel A.J. Effect of post annealing on CBD deposited ZnS thin films. *International Journal of Scientific Research and Reviews*, 2018, **7** (1), P. 374–384.

[18] Basha S.J., Khidhirbrahmendra V., et al. Structural, optical, magnetic and thermal investigations on Cr3+ ions doped ZnS nanocrystals by co-precipitation method. *Journal of Science: Advanced Materials and Devices*, 2019, **4**, P. 260–266.

[19] Cullity B.D., Stock S.R. *Element of X-ray Diffraction*, Addison-Wesley, Massachusetts, 1956, 99 p.

[20] Wang J., Hou S., et al. Ultra-rapid formation of ZnO hierarchical structures from dilution-induced supersaturated solutions. *Cryst. Eng. Comm.*, 2014, **16**, P. 7115–7123.

[21] The Materials Project. Materials Data on Zn(HO)$_2$ by Materials Project. United States, 2020. URL: https://doi.org/10.17188/1278479.

[22] Echendu O.K., Weerasinghe A.R., et al. Characterization of n-type and p-type ZnS thin layers grown by an electrochemical method. *Journal of Electronic Materials*, 2013, **42** (4), P. 692–700.

[23] Moholkar A.V., Agawane G.L., et al. Influence of deposition temperature on morphological, optical, electrical and opto-electrical properties of highly textured nano-crystalline spray deposited CdO:Ga thin films. *Applied Surface Science*, 2010, **257** (1), P. 93–101.

[24] Ruffner J.A., Himel M.D., et al. Effects of low substrate temperature and ion assisted deposition on composition, optical properties, and stress of ZnS thin films. *Applied Optics*, 1989, **28** (24), 5209.

[25] Ahn H., Um Y. Post-annealing effects on ZnS thin films grown by using CBD method. *Journal of Korean Physical Society*, 2015, **67** (6), P. 1045–1050.

[26] Nadeem M.Y., Ahmed W. Optical properties of ZnS thin films. *Turk. J. Phy.*, 2000, **24**, P. 651–659.

[27] Mendil R., Ben Ayadi Z., Ben Belgacem J., Djessas K. The properties of ZnS thin films prepared by rf-magnetron sputtering from nanoparticles synthesized by solvothermal/hydrothermal route. *J. Mater. Sci.: Mater. Electron.*, 2016, **27**, P. 444–451.

[28] Babu P., Reddy M., et al. Chemical bath deposition of Mn-doped ZnS thin films using greener complexing agents: Effect of Mn-doping on the optical properties. *Optik*, 2017, **130**, P. 608–618.

[29] Fairbrother A., Izquierdo-Roca V., et al. ZnS grain size effects on near-resonant Raman scattering: optical non-destructive grain size estimation. *Cryst. Eng. Comm.*, 2014, **16**, P. 4120–4125.

[30] Vishwakarma R. Effect of substrate temperature on ZnS films prepared by thermal evaporation technique. *J. Theor. Appl. Phys.*, 2015, **9**, P. 185–192.

[31] Shukla V., Patel A. Effect of doping concentration on optical and electrical properties of intrinsic n-type ZnO (i-ZnO) and (Cu,Na and K) doped p-type ZnO thin films grown by chemical bath deposition method. *Nanosystems: physıcs, chemıstry, mathematıcs*, 2020, **11** (4), P. 391–400.

[32] Göde F., Gümüş C. Influences of copper and manganese concentrations on the properties of polycrystalline ZnS:Cu and ZnS:Mn thin films. *Journal of Optoelectronics and Advanced Materials*, 2009, **11** (4), P. 429–436.